PAPER

A novel Au/electroactive poly(amic acid) composite as an effective catalyst for *p*-nitrophenol reduction†

Guan-Hui Lai, [ID] [a] Tsao-Cheng Huang,[b] Bi-Sheng Huang[a] and Yi-Chen Chou [ID] *[a]

A Au/electroactive poly(amic acid) (Au/EPAA) composite was synthesized and characterized, and its catalytic ability was evaluated. EPAA was synthesized *via* oxidative coupling polymerization and Au nanoparticles were anchored to the amino and carboxyl groups. The Au/EPAA composite was characterized *via* X-ray diffraction analysis, X-ray photoelectron spectroscopy, and scanning electron microscopy, which confirmed that the Au nanoparticles were well dispersed on the EPAA surface. *p*-Nitrophenol was reduced to *p*-aminophenol within 5 min at room temperature, with a rate constant of 0.84 min^{-1}. Cycling measurements showed that the Au/EPAA composite achieved higher than 92% conversion. The Au/EPAA composite showed excellent performance and stability as a catalyst for the reduction of *p*-nitrophenol to *p*-aminophenol.

1 Introduction

Increasing amounts of organic compounds are used in industry and produced daily; hence, water, as a commonly used solvent containing untreated organic agents or byproducts, is also generated continuously. Thus, proper treatment of wastewater has become an important issue. Heterogeneous catalysts based on metal nanoparticles (NPs) are promising tools for wastewater treatment. Typically, metal NPs are loaded onto a support such as carbon nanotube,[1] graphene,[2] boron nitride,[3] clay,[4] metal oxides,[5] or polymers[6] to prevent aggregation. Thus, improving the dispersion stability of metal NPs on a support is critical for the design and synthesis of high-performance heterogeneous catalysts.

Polymers are among the most popular catalyst support materials as they can stabilize metal NPs to prevent aggregation.[7,8] For example, Zhang *et al.* used an *in situ* method to prepare sulfhydryl-functionalized poly(glycidyl methacrylate) microspheres with surface sulfhydryl groups to adsorb Ag NPs. The sulfhydryl functional groups improved the monodispersity and recyclability of the Ag NPs in the catalyst system.[9] Liu *et al.* anchored Au NPs on thin carbon sheets to prepare highly stable and efficient heterogeneous catalysts. The Au/carbon sheets were synthesized using sol–gel, calcination, and selective etching methods and featured many amino functional groups

anchoring Au NPs stably on the surface.[10] Zhang *et al.* fabricated porous Au/polyethyleneimine/graphene oxide composites *via* an *in situ* deposition and freeze-drying method. Poly-ethyleneimine functioned not only as a reducing and protective agent for the Au NPs, but also as a reducing agent and surface modifier for graphene oxide. The resulting porous functional composite exhibited excellent catalytic activity for the reduction of *p*-nitrophenol (PNP).[11] In addition, Li has reported that dopamine-terminated poly(*N*-isopropylacrylamide)-modified carbon dots can easily anchor Au NPs on the material surface.[12] Functional groups with a lone pair, such as –NH, –SH, –COOH, and –OH groups, can effectively adsorb metal NPs on a carrier uniformly without agglomeration, but material synthesis requires several complex steps, making it expensive, time-consuming, and highly energy-consuming.[6,13,14]

Polyaniline (PANI) is used as a polymer support for Au NPs because it is relatively cheap, easy to synthesize, and effective for immobilization of Au NPs and has special doping/dedoping properties and conductivity.[15] However, it is difficult to dissolve in organic solvents, which limits its application. Thus, aniline oligomers and their derivative polymers have attracted attention because of their good solubility, mechanical strength, and biodegradability. Kaner *et al.* have demonstrated that tetraaniline is the smallest oligomer unit that can fully represent the structure of PANI, and single crystals of doped tetraaniline with different shapes can be produced through a simple self-assembly process.[16] Chao and Berda synthesized a series of electroactive polymers and showed that their electrochromic behaviors can be controlled by adjusting the pH and the applied potential.[17] Wang and co-workers prepared electroactive poly-mers containing aniline oligomers in the main and side chains, which exhibited electrochemical, dielectric, and

[a]Department of Cosmetic Science, Providence University, 43301 Taichung, Taiwan. E-mail: jacs1yichen@pu.edu.tw

[b]Technical Department Plastics Division, Formosa Plastics Corporation, 814538 Kaohsiung, Taiwan

† Electronic supplementary information (ESI) available. See DOI: 10.1039/d1ra05347g

photoresponsive properties.[18,19] Huang and co-workers investigated the anti-corrosion properties of electroactive polymers and attributed them to the passive metal oxide layers on the metal electrode surface induced by the redox catalytic capabilities of the aniline oligomer units in the electroactive polymer.[20–22] In addition, electroactive polymers have been utilized as sensing materials because of their unique properties, such as their acid–base properties, doping-dedoping chemistry, and redox behavior.[23–25]

In our previous studies, aniline oligomers and electroactive polymers incorporating graphene oxide, SiO_2, Au NPs, or carbon nanotubes were used as catalysts,[26] anti-corrosion coating materials,[27] and chemical sensors.[28,29] Poly(amic acid) (PAA), containing amide and carboxyl groups, is a typical precursor for polyimides. In this study, we synthesized electroactive PAA (EPAA) *via* oxidative coupling polymerization and anchored Au NPs directly on it *via* the amino and carboxyl groups in the polymer chain. This Au/EPAA composite was used to reduce PNP, one of the water pollutants prioritized by the US Environmental Protection Agency.[30] PNP is toxic to humans and animals, whereas the reduction product, *p*-aminophenol (PAP), is an important intermediate of paracetamol.[31]

2 Experimental

2.1 Materials

4,4′-Oxydiphthalic anhydride (ODPA, 98%, TCI), *N*-phenyl-*p*-phenylenediamine (98%, Aldrich), 1,4-phenylenediamine (99%, Aldrich), ammonium persulfate (APS, Aldrich), *N*-methyl-2-pyrrolidone (NMP, Tedia), dichloromethane (Tedia), hydrochloric acid (HCl, Showa), ammonium hydroxide (Showa), hydrazine (Acros), tetrachloroauric(III) acid trihydrate (Acros), sodium citrate (Aldrich), PNP (Aldrich), and sodium borohydride ($NaBH_4$, Aldrich) were obtained from various sources.

2.2 Synthesis of EPAA

2.2.1 Preparation of EPAA oligomers. The EPAA oligomer was synthesized by dissolving 0.62 g (2.0 mmol) of ODPA in 10 mL of NMP containing 4.0 mmol of *N*-phenyl-*p*-phenylenediamine. The solution was magnetically stirred for 4 h, and then 100 mL of deionized (DI) water was added to precipitate the EPAA oligomer. The EPAA oligomer was filtered, washed with excess DI water, and dried in a vacuum oven at 60 °C overnight before purification with dichloromethane. The calculated mass (m/z) for $C_{32}H_{26}N_4$ is 678.2 and a mass of 677.2 was found for this product (Fig. S1†). ^{1}H NMR spectroscopy of EPAA oligomers is shown in Fig. S2.†

2.2.2 Preparation of EPAA. EPAA was prepared (Fig. 1) by simultaneously dissolving 1.02 g (1.5 mmol) of the EPAA oligomer and 0.16 g (1.5 mmol) of 1,4-phenylenediamine in 30 mL of NMP with 1 mL (1.0 M) of HCl and stirring the resulting solution overnight. Subsequently, a solution containing 0.23 g (1.0 mmol) of APS was added dropwise while stirring at room temperature, and 100 mL of DI water was added to precipitate the dark green product. EPAA was washed with excess DI water several times and dried in a vacuum oven at 60 °C for 24 h. The
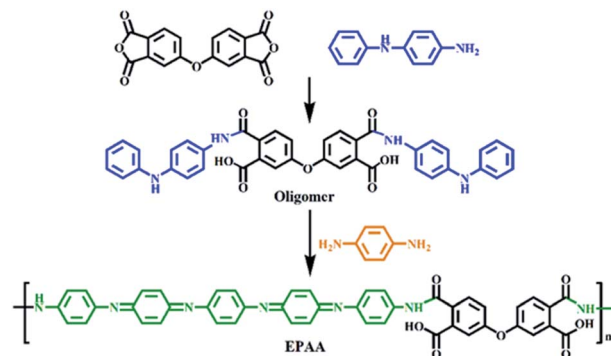

Fig. 1 Synthesis of EPAA.

number average molecular weight (M_n) was 9.82×10^4, the weight average molecular weight (M_w) was 1.25×10^5, and the polydispersity index was 1.28. ^{1}H NMR spectroscopy of EPAA is shown in Fig. S3.†

2.3 Synthesis of Au/EPAA composites

The Au NPs were prepared using the thermal reflux method. A solution of 0.0394 g (1.0 mM) of tetrachloroauric(III) acid trihydrate in 100 mL of DI water was heated, and 0.1141 g (38.8 mM) of sodium citrate was dissolved in 10 mL of DI water. After the solution had boiled, the sodium citrate solution was added and the resulting mixture was stirred for 10 min to obtain a solution of Au NPs. The Au/EPAA composite was prepared by dispersing 10 mg of EPAA in 50 mL of the Au NP solution and stirring overnight. The Au/EPAA composites were recovered *via* centrifugation at 6000 rpm for 10 min and washed three times with DI water.

2.4 Catalytic activity of the Au/EPAA composite

The catalytic properties of the Au/EPAA composite were monitored through ultraviolet-visible (UV-vis) spectroscopy *via* the conversion of PNP to PAP using $NaBH_4$ as a reductant. In a quartz cell, 3.0 mL of a PNP solution (1.0 mM) was mixed with 0.30 mL of a $NaBH_4$ solution (1.0 M), and the color of the solution changed from light yellow to dark yellow. The solution became colorless with the addition of 1.0 mg of the Au/EPAA composite.

2.5 Characterization

Liquid chromatography-mass spectra were obtained using a triple quadrupole mass spectrometer (TSQ Quantum) with an electrospray ionization source. The chemical structures of the oligomer and EPAA were determined *via* [1]H nuclear magnetic resonance (NMR) spectroscopy using a Bruker 400 spectrometer with deuterated dimethyl sulfoxide (DMSO-d_6) as the solvent. The weight average molecular weight (M_w) and number average molecular weight (M_n) were determined through gel permeation chromatography (GPC) using a Waters-150CV pump and a differential refractometer. Fourier-transform infrared (FTIR) spectroscopy was performed using a Jasco FT/IR-4600 spectrometer at room temperature with a resolution of 4 cm^{-1} and

64 scans. UV-vis spectroscopy was performed on a Jasco V-750 UV-visible spectrophotometer. Electrochemical experiments were performed on a CHI 6273E electrochemical analyzer using a Ag/AgCl reference electrode and Pt counter electrode at a scan rate of 50 mV s^{-1}. Thermogravimetric analysis (TGA) was conducted on a TA Instruments Q500 from 50 to 800 °C in air at a heating rate of 20 °C min^{-1}. X-ray diffraction (XRD) measurements were performed with a PANalytical X'Pert 3 powder diffractometer to investigate the crystalline structure of the Au NPs. X-ray photoelectron spectroscopy (XPS) was performed using a PHI 1600 ESCA spectrometer (Physical Electronics, Inc.). A JEOL JSM-7100F scanning electron microscope and JEM-1400 transmission electron microscope were employed to investigate the morphologies and structures of the typical products.

3 Results and discussion

Fig. 2(a) shows the FTIR spectra of the oligomer and EPAA between 4000 and 600 cm^{-1}; the characteristic N–H and O–H peaks were observed at 3500–3200 cm^{-1}. The peaks at 1711, 1311, and 744 cm^{-1} correspond to C=O symmetric stretching, C–N bending, and C–H bending, respectively.[32] The peaks at 1589 and 1509 cm^{-1} correspond to N=Q=N and N=B=N bonding, where Q represents the quinoid ring and B represents the benzene ring structure.[33,34] The chemical oxidation of EPAA is shown in Fig. 2(b). The obtained EPAA (0.4 g) was dispersed in a solution of 4 mL of hydrazine hydrate in 40 mL of 1.0 M ammonium hydroxide and the resulting mixture was stirred for 10 h. The reaction mixture was then filtered, and the residue was washed with distilled water several times and dried under dynamic vacuum at 40 °C for 24 h. Finally, EPAA was reduced to the leucoemeraldine oxidation state (0.34 g, 85%). The leucoemeraldine base (LB) form of EPAA was dissolved in NMP. Subsequently, trace amounts of the oxidant, $(NH_4)_2S_2O_8$, were gradually introduced into the EPAA solution for *in situ* monitoring of the sequential oxidation of the conjugated aniline

Fig. 3 (a) UV-vis spectra of Au and Au/EPAA composite. (b) XRD patterns of EPAA and Au/EPAA composite. (c) XPS spectra of EPAA and the Au/EPAA composite; (d) high-resolution Au 4f XPS spectrum of the Au/EPAA composite.

pentamer components through UV-vis absorption spectroscopy. The LB form gave only one absorption peak at 310 nm, which is associated with the π–π* transition of the conjugated ring system.[35] During oxidation, this absorption peak of EPAA was blue-shifted to 297 nm. A new absorption peak was observed at 591 nm, which was assigned to the benzenoid-to-quinoid excitonic transition.[36] Cyclic voltammetry (CV) studies have been used to examine the redox properties of electroactive polymers. In this study, EPAA was examined using CV with a typical three-electrode electrochemical cell. As shown in Fig. 2(c), the CV curve shows redox peaks for EPAA at 0.37, 0.51, and 0.70 V.[37] Fig. 2(d) shows that EPAA starts in the LB state containing a benzene ring, and is oxidized to emeraldine base I (EB I), then
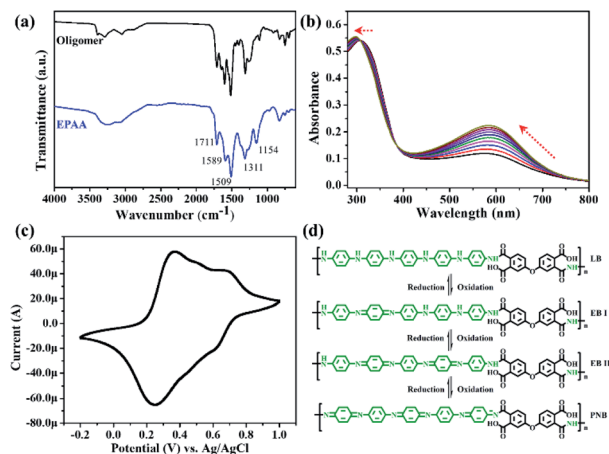

Fig. 2 (a) FTIR spectra of oligomer and EPAA. (b) UV-vis spectra monitoring chemical oxidation of EPAA. (c) CV measurements for EPAA. (d) Redox states of EPAA.
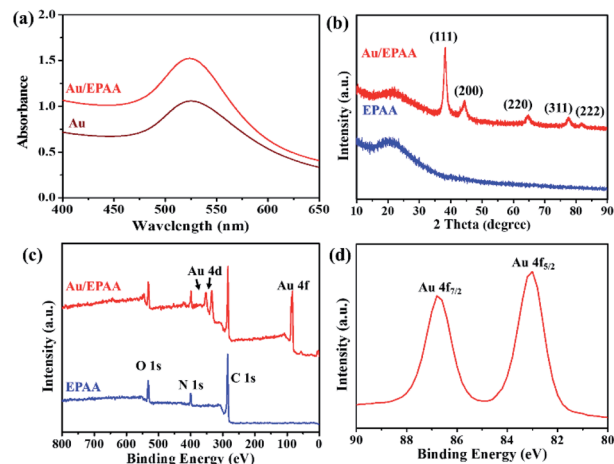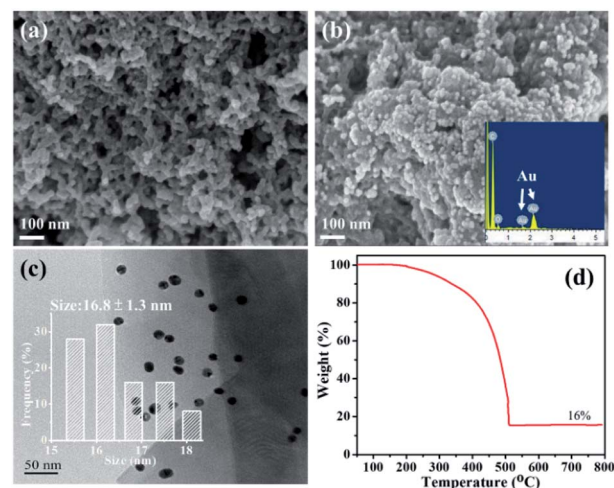

Fig. 4 Scanning electron microscopy (SEM) images of (a) EPAA and (b) Au/EPAA; the insert shows the energy dispersive X-ray spectroscopy (EDS) spectrum of the Au/EPAA composite. (c) TEM image of Au/EPAA; the insert shows the particle size distribution. (d) TGA results for the Au/EPAA composite.
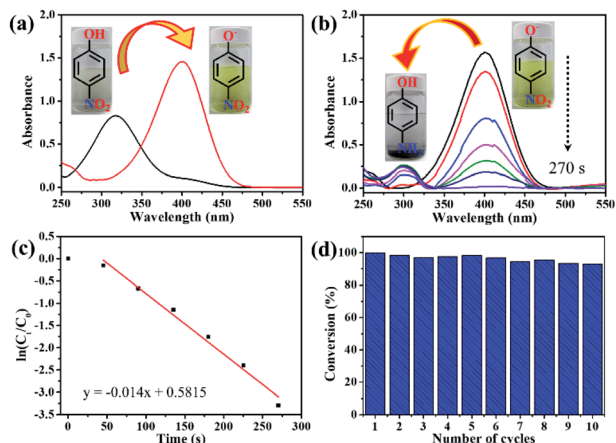
Fig. 5 UV-vis spectra of (a) PNP before and after adding $NaBH_4$ and (b) reduction of PNP with $NaBH_4$ using Au/EPAA composite. (c) Linear relationship between $\ln(C_t/C_0)$ and reaction time with Au/EPAA composite as a catalyst. (d) Cycling performance of Au/EPAA composite for PNP reduction.

to emeraldine base II (EB II), and finally to the pernigraniline base (PNB), with the quinoid ring peak (591 nm) growing until equilibrium is reached.

When gold is nanometer-sized, there is a special plasma resonance effect.[38] The peak at 523 nm in the UV-vis spectrum corresponded to Au NPs approximately 15 nm in size,[39] as shown in Fig. 3(a). The morphologies of the Au NPs were examined through their transmission electron microscopy (TEM) images, and their diameter was 15.8 ± 1.7 nm (Fig. S4†). After the Au NPs were adsorbed on the EPAA surface to afford the Au/EPAA composite, the peak remained at 524 nm. The crystallinities of EPAA and the Au/EPAA composite were investigated using XRD, and the results are shown in Fig. 3(b). The broad peak at 20.5° indicates the amorphous phase in the EPAA polymer. For the Au/EPAA composite, the diffraction peaks at 38.2°, 44.4°, 64.8°, 77.7°, and 81.8° can be ascribed to the (111), (200), (220), (311), and (222) crystal planes of Au, respectively.[40–42] The XPS survey spectra of EPAA and the Au/EPAA composite are shown in Fig. 3(c). EPAA gave significantly intense C 1s, N 1s, and O 1s peaks at 284.30, 399.81, and

531.43 eV, respectively.[43] After the adsorption of Au NPs, the Au/EPAA composite gave an additional Au 4f peak, which was attributed to the anchoring of Au NPs on EPAA, confirming successful adsorption. The peaks at binding energies of 86.79 and 82.99 eV in Fig. 3(d) can be attributed to Au $4f_{7/2}$ and Au $4f_{5/2}$, respectively, confirming the loading of Au NPs on the surface of EPAA.[44]

The morphologies of EPAA and the Au/EPAA composites are shown in Fig. 4(a–c). Au NPs can be clearly observed in the image of the Au/EPAA composite, but not in that of EPAA, which showed that the Au NPs were well dispersed. The TEM image of the Au/EPAA composite shows that the Au NPs are well dispersed on the EPAA surface with an average size of 16.8 ± 1.3 nm (Fig. 4(c)). Fig. 4(d) displays the TGA results for the Au/EPAA composite. To the best of our knowledge, the polymer decomposes into CO and CO_2 when heated to 800 °C in air. With the anchored Au NPs, the combustion residue of the Au/EPAA composite had 16% of the initial weight owing to the Au NP content.

The catalytic activity of the Au/EPAA composite for the reduction of PNP to PAP with $NaBH_4$ was evaluated. When $NaBH_4$ was added, the peak for PNP shifted from 317 to 400 nm, indicating the formation of p-nitrophenolate ions, as shown in Fig. 5(a). This reaction did not occur in the absence of the catalyst. Fig. 5(b) displays the typical UV-spectra at 300 nm,[45] which show the formation of PAP from the reduction of the p-nitrophenolate ion.[46] After the Au/EPAA composite was added, the solution changed from dark yellow to colorless, and the reduction reaction was completed within 270 s without ultrasound or stirring. This behavior was expected because the Au
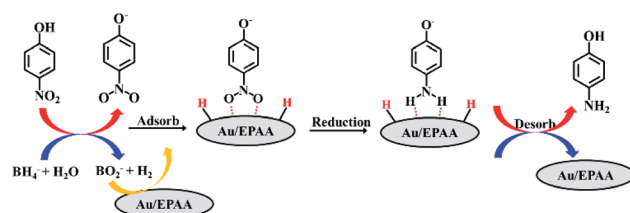

Fig. 6 Mechanism for reduction of PNP.

Table 1 Comparison of catalysts for the reduction of PNP in the presence of $NaBH_4$

Catalyst	Weight (mg)	Reduction time (s)	Rate constant (min^{-1})	4-NP : $NaBH_4$	Conversion	Ref.
Fe_3O_4–Cu	0.2	15	NA	1 : 40	90%, 6 times	50
Fe_3O_4–Au	NA	120	1.82	1 : 40	>90%	51
Au/EPAA	1.0	270	0.84	1 : 100	>92%, 10 times	This work
Au@S-g-$C_3N_4{}^a$	2.5	300	0.75	1 : 100	95%, 5 times	52
PdO/ZnO	1	360	0.37	1 : 100	>93%, 5 times	49
$HMSC^b$–NiCoP	100	585	2.24	1 : 100	97%, 6 times	53
PtNi/RGO^c	0.05	600	6.48	1 : 2380	86%, 5 times	54
Ag@NC^d	1	840	0.25	1 : 1250	>90%, 5 times	55

^{a} S-g-C_3N_4: sulfur doped graphitic carbon nitride. ^{b} HMSC: hollow microsphere supported. ^{c} RGO: reduced graphene oxide. ^{d} NC: nanoporous carbon.

NPs in the Au/EPAA composites adsorb hydrogen from $NaBH_4$ and efficiently release it *via* reduction. Hence, Au NPs act as hydrogen carriers between $NaBH_4$ and PNP. Since the concentration of $NaBH_4$ exceeded that of PNP, this reduction reaction can be assumed to be a pseudo-first-order reaction that can be described as follows:[47]

$$\ln(C_t/C_0) = -kt$$

where C_0 is the initial concentration, C_t is the concentration at time t, and k is the rate constant. The linear relationship between $\ln(C_t/C_0)$ and the reaction time shown in Fig. 5(c) is consistent with first-order reaction kinetics. From this kinetic curve, the rate constant k with the Au/EPAA composite was determined to be 0.84 min^{-1}. Another evaluation index of the catalyst ability for the reduction of PNP is the stability and recyclability of the catalyst. Therefore, we examined the reusability of the Au/EPAA composite over ten cycles (Fig. 5(d)). At the end of each reduction reaction, the Au/EPAA composite was collected *via* centrifugation and washed thoroughly with DI water for the next cycle. After ten cycles, PNP conversion was still higher than 92%, indicating the high stability of the synthesized catalyst. This shows that the Au NPs are stabilized on the EPAA surface. Compared to other metallic-NP-based catalysts (Table 1), the Au/EPAA composite exhibited high catalytic activity, confirming its potential for practical application.[38–44]

The mechanism for the reduction of PNP using the Au/EPAA composite can be described using the Langmuir–Hinshelwood model.[47–49] The PNP and BH_4^- ions are first adsorbed on the surface of the Au/EPAA composite, where BH_4^- acts as a hydrogen source. Then, the *p*-nitrophenolate ion is converted into a *p*-aminophenolate ion *via* the transfer of hydrogen and electrons. Finally, PAP is desorbed from the surface of the Au/EPAA composite, as shown in Fig. 6. At the same time, the Au/EPAA composite returns to its initial state to maintain stability.

4   Conclusions

In conclusion, a new Au/EPAA composite was synthesized to catalyze the reduction of PNP to PAP. Au NPs were anchored and well dispersed on the EPAA surface *via* the carboxyl and amino groups of EPAA. This Au/EPAA composite exhibited excellent catalytic properties for the reduction of PNP, with a rate constant of 0.84 min^{-1}. After ten cycles, the conversion with Au/EPAA was still higher than 92%. The Au/EPAA composite exhibited high catalytic activity; hence, it has potential for new applications.

Author contributions

Guan-Hui Lai: conceptualization, methodology, investigation, data curation, writing – original draft. Tsao-Cheng Huang: methodology, supervision, writing – review & editing. Bi-Sheng Huang: investigation, data curation. Yi-Chen Chou: writing – review & editing, supervision, project administration, funding acquisition.

Conflicts of interest

There are no conflicts to declare.

Acknowledgements

References

1 X. Gu, W. Qi, X. Xu, Z. Sun, L. Zhang, W. Liu, X. Pan and D. Su, *Nanoscale*, 2014, **6**, 6609–6616.
2 X.-Y. Zhu, Z.-S. Lv, J.-J. Feng, P.-X. Yuan, L. Zhang, J.-R. Chen and A.-J. Wang, *J. Colloid Interface Sci.*, 2018, **516**, 355–363.
3 B. Yu, B. Han, X. Jiang, C. Zhou, K. Xia, Q. Gao and J. Wu, *J. Phys. Chem. C*, 2019, **123**, 10389–10397.
4 G.-H. Lai, T.-C. Huang, Y.-H. Pai, B.-S. Huang, M.-H. Tsai, T.-I. Yang and Y.-H. Chung, *J. Taiwan Inst. Chem. Eng.*, 2019, **95**, 525–531.
5 Y. Xu, X. Shi, R. Hua, R. Zhang, Y. Yao, B. Zhao, T. Liu, J. Zheng and G. Lu, *Appl. Catal., B*, 2020, **260**, 118142.
6 B. Hao, G. Lu, S. Zhang, Y. Li, A. Ding and X. Huang, *Polym. Chem.*, 2020, **11**, 4094–4104.
7 Q. Geng and J. Du, *RSC Adv.*, 2014, **4**, 16425–16428.
8 R. Rarima and G. Unnikrishnan, *Mater. Chem. Phys.*, 2020, **241**, 122389.
9 W. Zhang, Y. Sun and L. Zhang, *Ind. Eng. Chem. Res.*, 2015, **54**, 6480–6488.
10 X. Liu, X. Cui, Y. Liu and Y. Yin, *Nanoscale*, 2015, **7**, 18320–18326.
11 P. Deng, Z. Xu, Y. Feng and J. Li, *Sens. Actuators, B*, 2012, **168**, 381–389.
12 L. Li, T. Zhang, J. Lü and C. Lü, *Appl. Surf. Sci.*, 2018, **454**, 181–191.
13 J. Zhou, C. Zhang and Y. Wang, *Polym. Chem.*, 2019, **10**, 1642–1649.
14 G. Wu, X. Liu, P. Zhou, L. Wang, M. Hegazy, X. Huang and Y. Huang, *Mater. Sci. Eng., C*, 2019, **94**, 524–533.
15 X. Feng, C. Mao, G. Yang, W. Hou and J.-J. Zhu, *Langmuir*, 2006, **22**, 4384–4389.
16 Y. Wang, H. D. Tran, L. Liao, X. Duan and R. B. Kaner, *J. Am. Chem. Soc.*, 2010, **132**, 10365–10373.
17 Y. Wang, X. Jia, E. B. Berda, J. Zhao, X. Liu and D. Chao, *Eur. Polym. J.*, 2020, **138**, 109979.
18 Y. Yan, N. Sun, X. Jia, X. Liu, C. Wang and D. Chao, *Polymer*, 2018, **134**, 1–7.
19 Y. Yan, N. Sun, F. Li, X. Jia, C. Wang and D. Chao, *ACS Appl. Mater. Interfaces*, 2017, **9**, 6497–6503.
20 H.-Y. Huang, T.-C. Huang, J.-C. Lin, J.-H. Chang, Y.-T. Lee and J.-M. Yeh, *Mater. Chem. Phys.*, 2013, **137**, 772–780.

21 T.-C. Yeh, T.-C. Huang, H.-Y. Huang, Y.-P. Huang, Y.-T. Cai, S.-T. Lin, Y. Wei and J.-M. Yeh, *Polym. Chem.*, 2012, **3**, 2209–2216.

22 T. C. Huang, J. M. Yeh and C. Y. Lai, in *Advances in Polymer Nanocomposites*, ed. F. Gao, Woodhead Publishing, 2012, pp. 605–638.

23 T. C. Huang, L. C. Yeh, G. H. Lai, F. Y. Lai, T. I. Yang, Y. J. Huang, A. Y. Lo and J. M. Yeh, *eXPRESS Polym. Lett.*, 2016, **10**, 450–461.

24 L.-C. Yeh, T.-C. Huang, Y.-P. Huang, H.-Y. Huang, H.-H. Chen, T.-I. Yang and J.-M. Yeh, *Electrochim. Acta*, 2013, **94**, 300–306.

25 L.-C. Yeh, T.-C. Huang, F.-Y. Lai, G.-H. Lai, A.-Y. Lo, S.-C. Hsu, T.-I. Yang and J.-M. Yeh, *Surf. Coat. Technol.*, 2016, **303**, 154–161.

26 G.-H. Lai, Y.-C. Chou, B.-S. Huang, T.-I. Yang and M.-H. Tsai, *RSC Adv.*, 2021, **11**, 71–77.

27 Y.-C. Chou, P.-C. Lee, T.-F. Hsu, W.-Y. Huang, L. Zi-Han, C.-Y. Chuang, T.-I. Yang and J.-M. Yeh, *Polym. Compos.*, 2014, **35**, 617–625.

28 T.-C. Huang, L.-C. Yeh, H.-Y. Huang, Z.-Y. Nian, Y.-C. Yeh, Y.-C. Chou, J.-M. Yeh and M.-H. Tsai, *Polym. Chem.*, 2014, **5**, 630–637.

29 M. H. Tsai, S. H. Lu, Y. H. Lai, G. H. Lai, G. V. Dizon, T. I. Yang, Y. J. Lin and Y. C. Chou, *eXPRESS Polym. Lett.*, 2018, **12**, 71–81.

30 S. A. Hira, M. Nallal and K. H. Park, *Sens. Actuators, B*, 2019, **298**, 126861.

31 M. T. Islam, N. Dominguez, M. A. Ahsan, H. Dominguez-Cisneros, P. Zuniga, P. J. J. Alvarez and J. C. Noveron, *J. Environ. Chem. Eng.*, 2017, **5**, 4185–4193.

32 T.-C. Huang, S.-T. Lin, L.-C. Yeh, C.-A. Chen, H.-Y. Huang, Z.-Y. Nian, H.-H. Chen and J.-M. Yeh, *Polymer*, 2012, **53**, 4373–4379.

33 T.-C. Huang, L.-C. Yeh, G.-H. Lai, B.-S. Huang, T.-I. Yang, S.-C. Hsu, A.-Y. Lo and J.-M. Yeh, *Int. J. Green Energy*, 2017, **14**, 113–120.

34 H.-Y. Huang, J.-W. Jian, Y.-T. Lee, Y.-T. Li, T.-C. Huang, J.-H. Chang, L.-C. Yeh and J.-M. Yeh, *Polymer*, 2012, **53**, 4967–4976.

35 R. Yang, D. Chao, H. Liu, E. B. Berda, S. Wang, X. Jia and C. Wang, *Electrochim. Acta*, 2013, **93**, 107–113.

36 T.-C. Huang, T.-C. Yeh, H.-Y. Huang, W.-F. Ji, T.-C. Lin, C.-A. Chen, T.-I. Yang and J.-M. Yeh, *Electrochim. Acta*, 2012, **63**, 185–191.

37 T.-C. Huang, T.-C. Yeh, H.-Y. Huang, W.-F. Ji, Y.-C. Chou, W.-I. Hung, J.-M. Yeh and M.-H. Tsai, *Electrochim. Acta*, 2011, **56**, 10151–10158.

38 T. Wu, Y. Kou, H. Zheng, J. Lu, N. R. Kadasala, S. Yang, C. Guo, Y. Liu and M. Gao, *Nanomaterials*, 2020, **10**, 48.

39 N. G. Bastús, J. Comenge and V. Puntes, *Langmuir*, 2011, **27**, 11098–11105.

40 S. S. Kumar, C. S. Kumar, J. Mathiyarasu and K. L. Phani, *Langmuir*, 2007, **23**, 3401–3408.

41 T. Wu, H. Zheng, Y. Kou, X. Su, N. R. Kadasala, M. Gao, L. Chen, D. Han, Y. Liu and J. Yang, *Microsyst. Nanoeng.*, 2021, **7**, 23.

42 J.-M. Yeh, K.-Y. Huang, S.-Y. Lin, Y.-Y. Wu, C.-C. Huang and S.-J. Liou, *J. Nanotechnol.*, 2009, **2009**, 217469.

43 H. Yao, T.-C. Huang and H.-J. Sue, *RSC Adv.*, 2014, **4**, 61823–61830.

44 M.-Q. Yang, X. Pan, N. Zhang and Y.-J. Xu, *CrystEngComm*, 2013, **15**, 6819–6828.

45 H. Zheng, J. Huang, T. Zhou, Y. Jiang, Y. Jiang, M. Gao and Y. Liu, *Catalysts*, 2020, **10**, 1437.

46 Q. Cheng, Q. Li, Z. Yuan, S. Li, J. H. Xin and D. Ye, *ACS Appl. Mater. Interfaces*, 2021, **13**, 4410–4418.

47 S. K. Ghosh, M. Mandal, S. Kundu, S. Nath and T. Pal, *Appl. Catal., A*, 2004, **268**, 61–66.

48 L. Qin, Z. Zeng, G. Zeng, G. Lai, A. Duan, R. Xiao, D. Huang, Y. Fu, H. Yi, B. Li, X. Liu, S. Liu, M. Zhang and D. Jiang, *Appl. Catal., B*, 2019, **259**, 118035.

49 M. Liu, F. Cui, Q. Ma, L. Xu, J. Zhang, R. Zhang and T. Cui, *New J. Chem.*, 2020, **44**, 4042–4048.

50 W. Zhao, S. Yang, C. Guo, J. Yang and Y. Liu, *Mater. Chem. Phys.*, 2021, **260**, 124144.

51 Y. Chen, T. Wu, G. Xing, Y. Kou, B. Li, X. Wang, M. Gao, L. Chen, Y. Wang, J. Yang, Y. Liu, Y. Zhang and D. Wang, *Ind. Eng. Chem. Res.*, 2019, **58**, 15151–15161.

52 V. Balakumar, H. Kim, J. W. Ryu, R. Manivannan and Y.-A. Son, *J. Mater. Sci. Technol.*, 2020, **40**, 176–184.

53 G. Du, B. Liao, R. Liu, Z. An and J. Zhang, *RSC Adv.*, 2020, **10**, 35287–35294.

54 P. Song, J.-J. Feng, S.-X. Zhong, S.-S. Huang, J.-R. Chen and A.-J. Wang, *RSC Adv.*, 2015, **5**, 35551–35557.

55 V. Veeramani, N. Van Chi, Y.-L. Yang, N. T. Hong Huong, T. Van Tran, T. Ahamad, S. M. Alshehri and K. C. W. Wu, *RSC Adv.*, 2021, **11**, 6614–6619.